

Article pubs.acs.org/JPCB

## Theory of Protein Charge Transfer: Electron Transfer between Tryptophan Residue and Active Site of Azurin

Published as part of The Journal of Physical Chemistry virtual special issue "Pablo G. Debenedetti Festschrift". Setare Mostajabi Sarhangi and Dmitry V. Matyushov\*



Cite This: J. Phys. Chem. B 2022, 126, 10360-10373



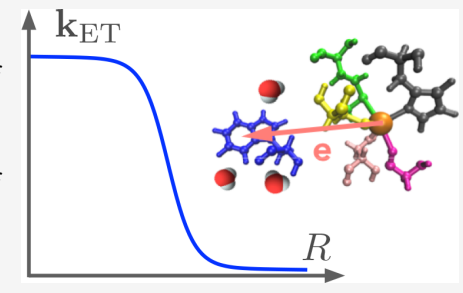
**ACCESS** I

III Metrics & More

Article Recommendations

Supporting Information

ABSTRACT: One reaction step in the conductivity relay of azurin, electron transfer between the Cu-based active site and the tryptophan residue, is studied theoretically and by classical molecular dynamics simulations. Oxidation of tryptophan results in electrowetting of this residue. This structural change makes the free energy surfaces of electron transfer nonparabolic as described by the Qmodel of electron transfer. We analyze the medium dynamical effect on protein electron transfer produced by coupled Stokes-shift dynamics and the dynamics of the donor-acceptor distance modulating electron tunneling. The equilibrium donor-acceptor distance falls in the plateau region of the rate constant, where it is determined by the protein-water dynamics, and the probability of electron tunneling does not affect the rate. The crossover distance found here puts most



intraprotein electron-transfer reactions under the umbrella of dynamical control. The crossover between the medium-controlled and tunneling-controlled kinetics is combined with the effect of the protein-water medium on the activation barrier to formulate principles of tunability of protein-based charge-transfer chains. The main principle in optimizing the activation barrier is the departure from the Gaussian-Gibbsian statistics of fluctuations promoting activated transitions. This is achieved either by incomplete (nonergodic) sampling, breaking the link between the Stokes-shift and variance reorganization energies, or through wetting-induced structural changes of the enzyme's active site.

#### **■ INTRODUCTION**

Proteins are increasingly viewed as charge conducting media. 1-4 The reason for conductivity is sought in chains of aromatic residues that can be oxidized and serve as relay elements to direct oxidizing electron holes to the protein surface to avoid oxidative damage to active sites of enzymes. 5-9 Each hop in this sequence is viewed as a single electrontransfer step 10 as traditionally described by Marcus theory of electron transfer. 11 This article reports molecular dynamics (MD) simulations and theoretical modeling of a single step in such a relay involving electron transfer between the active site of azurin protein (Figure 1, PDB 1AZU) and the nearby tryptophan residue as studied experimentally by Shih et al.<sup>6</sup>

The success of Marcus theory 11 in describing electron transfer is based on a generic mechanistic picture, applicable to many specific problems, in which the quantum system of the transferring electron is linearly coupled to a harmonic bath characterized by Gaussian statistics of fluctuations. The coupling strength changes between two electronic states, and that alters the equilibrium value of the collective medium coordinate q specified by minimizing the free-energy function

$$R_e \simeq 9.2-10.3~{
m \AA}$$

Figure 1. Drawing of the Cu-ligated active site and the tryptophan (Trp) residue of azurin (PDB 1AZU). The distance between Cu and the center of mass of the indole ring of Trp is  $R_{\varepsilon} = 9.2$  Å for the neutral Trp state and 10.3 Å for the cation radical state Trp+.

 $E_i(q) = -C_i q + \frac{1}{2} \kappa q^2$ 





(1)

Received: July 25, 2022

Published: December 2, 2022

October 29, 2022

Revised:

The second term in this equation arises from the truncated series expansion of the medium free energy in the deviation of the medium coordinate from its equilibrium value and denoted as q. Both the coupling constant  $C_i$  and the force constant  $\kappa$  depend on the thermodynamic state of the medium, thus the free-energy character of the functions  $E_i(q)$ . The physical meaning of the coordinate q is not specified here: it can be an actual collective vibration of the medium or the medium polarization considered in Marcus theory  $^{12}$  (with corresponding generalization to three dimensions, see below). Any complex medium with Gaussian statistics can be mapped on a manifold of harmonic oscillators with distributed vibrational frequencies.  $^{13,14}$  An extension  $q \rightarrow q_j$ ,  $\kappa \rightarrow \kappa_j$  allows such a mapping to which the arguments presented here fully apply.

Mathematically, the problem of finding the free energy (reversible work) required to bring two localized electronic states in tunneling resonance becomes equivalent to a mechanical problem of a harmonic spring pulled with an external Hookean force  $C_iq$  (Figure 2). Importantly, the

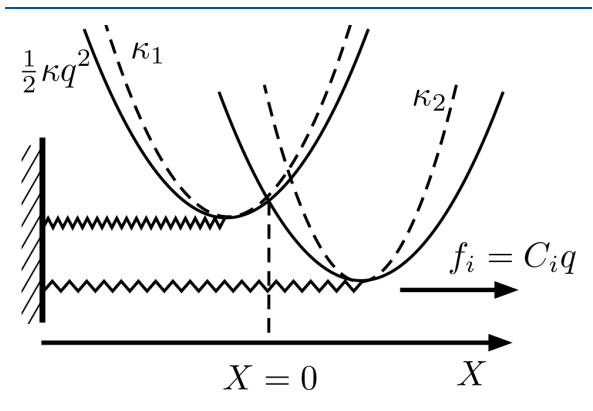


**Figure 2.** Mechanistic picture of Marcus model representing electron-transfer activation as a harmonic spring stretched by the external force  $f_i = C_i q$ . Thermal fluctuations of the spring extension are projected on the energy-gap reaction coordinate X with X=0 representing the tunneling configuration of resonance between the donor and acceptor electronic states. The dashed curves indicate parabolas with state-dependent curvatures specific to protein electron transfer with different wetting patterns of the active site in two oxidation states.

external force does not alter the force constant of the spring, implying the regime of linear deformation or linear response in statistical formulations of the theory. <sup>14</sup>

For electron transfer in polar liquids and proteins, the requirement of an invariant force constant  $\kappa$  physically implies that the structure of the medium is not altered by the transferring electron. This is not true for electron transfer between ions in solution where the local structure of the solvation shell is strongly affected by the ionic charge. However, the long range of the Coulomb interaction involves many solvent molecules from less perturbed solvation layers and, on average, the assumption a harmonic medium with an unperturbed force constant holds reasonably well.

Does this picture extend to protein electron transfer? Proteins are highly packed media with little room in their cores for structural changes induced by a single charge. The assumptions of the standard mechanistic model seem to apply here as well. There is one potential complication though not accounted for by the model of a structurally unperturbed protein core. Water is a light and mobile part of the thermal

bath that can respond to altering charge distribution by wetting parts of the protein core (electrowetting). There is increasing evidence, mostly from computer simulations, <sup>15–18</sup> that water can penetrate into active sites of redox-active proteins in response to a changing oxidation state. When this happens, the protein—water thermal bath changes its structure between two oxidation states and the force constant becomes state-dependent (dashed lines in Figure 2). One obtains the free-energy functions of the form

$$E_i(q) = -C_i q + \frac{1}{2} \kappa_i q^2 \tag{2}$$

The transition from eq 1 to eq 2 dramatically alters the description of activated dynamics for electron transfer. The standard formulation due to Warshel<sup>19</sup> views the vertical difference of energies, taken at the same value of the nuclear coordinate q, as the electron-transfer reaction coordinate

$$X = E_2(q) - E_1(q) (3)$$

For the standard Marcus description,  $X = \Delta Cq$  ( $\Delta C = C_2 - C_1$ ) is a linear function of q. The Gaussian statistics of q is projected onto the Gaussian statistics of X. This is mathematically expressed in terms of free energy surfaces of electron transfer  $F_i(X)$ , which carry the meaning of potentials of mean force along the single collective reaction coordinate X incorporating nuclear coordinates of multiple particles of the medium.  $C_{X,i}^{19-21}$  For the Gaussian distribution of  $C_{X,i}$  the functions  $C_{X,i}^{19-21}$  become parabolas with the Gaussian variance  $C_{X,i}^{20-1}$ 

$$\beta F_i(X) = \frac{(X - X_i)^2}{2\sigma_{X,i}^2} \tag{4}$$

where  $\beta = (k_{\rm B}T)^{-1}$  is the inverse temperature. The parabolas' minima are at  $X_{ij}$  and they cross at zero energy gap X=0 where tunneling occurs. The crossing point defines the Marcus activation energy for protein electron transfer. As described below, the use of Gibbsian statistics to calculate  $F_i(X)$  requires  $\sigma_{X,1} = \sigma_{X,2}$  in eq 4.

The situation changes when the force constants  $\kappa_i$  become unequal between two electron-transfer states. The energy gap is now a linear-quadratic function of q,  $X = -\Delta Cq + (\Delta \kappa/2)q^2$ ,  $\Delta \kappa = \kappa_2 - \kappa_1$ , and the Gaussian statistics of q is projected on non-Gaussian statistics of X. This problem has an exact solution through the Q-model of electron transfer<sup>22</sup> explained in more detail below. This mathematical formalism is directly applicable to the problem of electron transfer between the active site of azurin and the tryptophan (Trp) residue next to it. This kinetic step is a part of the charge-transfer relay delivering holes, initiated by photoexcitation, from the protein surface to the active site. 6 Molecular dynamics (MD) simulations presented below show that creation of a positive charge at Trp, by hole transfer, strongly alters its wetting by hydration water. The qualitative picture is illustrated in Figure 3 showing the density map of water molecules within 6 Å cutoff distance from the center of Trp in the neutral and oxidized states. The neutral state is hydrophobic,<sup>23</sup> while the cation radical Trp+ is hydrated. The wetting pattern depends on the charge distribution adopted for Trp+ (see Supporting Information (SI) for details), confirming the electrowetting mechanism. As a result, the structure of the protein-water medium is not the same in two electron-transfer states, and the standard Marcus framework does not apply. While formal mapping on the linear-quadratic function in eq 2 is still

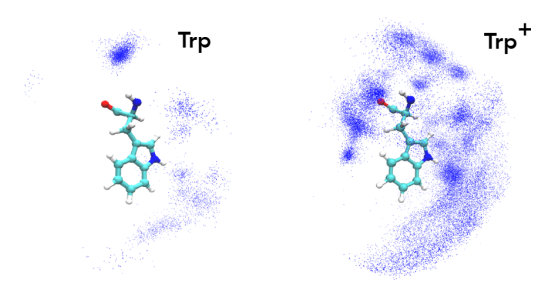


**Figure 3.** Water density map around Trp calculated from 30 ns of the MD simulation trajectory. Points in the map indicate appearances of water molecules within the cutoff distance of 6 Å from the center of neutral Trp and cation radical Trp<sup>+</sup>.

possible, the altering curvature of the parabola along the *q*-coordinate reflects the appearance of additional medium coordinates describing the extent of wetting. This more complex medium is still described by Gaussian statistics, which justifies the parabolic approximation.

The effect of medium dynamics on electron transfer gains in significance when switching from reactions between molecules in polar liquids to proteins. The general phenomenology of electron transfer controlled by medium dynamics<sup>24–27</sup> suggests a turnover from tunneling at longer distances, when the rate constant decays exponentially with the donor—acceptor separation, to the distance-independent rate, controlled by polarization dynamics, at shorter distances. The golden-rule expression for the reaction rate gives the rate constant pre-exponential factor in terms of the electronic coupling

$$V = V_{\varepsilon} \exp\left[-\frac{1}{2}\gamma \delta R\right] \tag{5}$$

where  $\gamma$  is the inverse decay length of tunneling and the distance is measured relative to the equilibrium donor–acceptor separation  $R_{e}$ ,  $\delta R=R-R_{e}$ . The expression for the rate constant in the golden-rule limit (nonadiabatic rate constant, NA) becomes  $^{28}$ 

$$k_{\rm NA} = v^2 \, \mathrm{e}^{1/2\gamma^2 \langle (\delta R)^2 \rangle - \beta \Delta F^\dagger} \tag{6}$$

where  $\Delta F^{\dagger}$  is the activation barrier and  $v^2 = (V_e^2/\hbar) \left[\pi \beta/\lambda\right]^{1/2}$  includes the reorganization energy of electron transfer  $\lambda$  (see below for a precise definition);  $\hbar$  is the Planck constant. The exponential factor  $(\gamma^2/2)\langle(\delta R)^2\rangle$  in this equation accounts for the statistical modulation of the electronic coupling by donor–acceptor displacements. <sup>28,29</sup>

The overall rate constant of electron transfer  $k_{\rm ET}$  including the dynamical medium effects follows from dividing  $k_{\rm NA}$  by the term  $1+sv^2$  to account for the effect of the medium dynamics  $^{25,26,28,29}$ 

$$k_{\rm ET} = \frac{v^2}{1 + sv^2} e^{1/2\gamma^2 \langle (\delta R)^2 \rangle - \beta \Delta F^{\dagger}}$$
(7)

The crossover parameter  $g=sv^2\propto v^2\propto \tau_X$  (s is the coefficient specified below) in the denominator grows quadratically with the electronic coupling  $V_e$  and linearly with the Stokes-shift relaxation time  $\tau_X$  when the polarization dynamics is the only mechanism of the medium dynamical effect. Lowering the donor—acceptor distance increases  $g=sv^2$  in the denominator of eq 7 such that the rate constant turns to a distance-independent plateau  $k_{\rm ET}\simeq k_{\rm max}$  at a sufficiently short distance.

The turnover distance  $R^*$  is reached at  $g(R^*) = 1$  at which the rate constant is equal to a half of its plateau value (Figure 4).

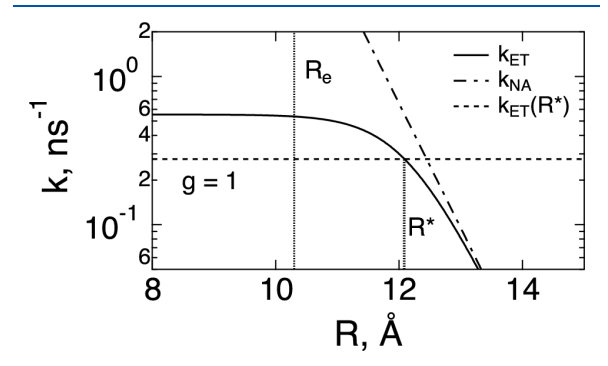


**Figure 4.** Rate constant of electron transfer vs the distance between the Cu atom of the active site and the center of mass of the indole ring of Trp (Figure 1). Shown are the nonadiabatic rate constant  $k_{\rm NA}$  (eq 6, dash-dotted line) and the electron-transfer rate constant  $k_{\rm ET}$  (eq 7, solid line) for the reaction of Trp+ reduction. The horizontal dashed line shows  $g(R^*)=1$ ,  $R^*=12.1$  Å, and the vertical dotted line indicates the equilibrium distance  $R_\varepsilon=\langle R\rangle=10.3$  Å from MD trajectories.

The turnover distance  $R^*$  depends on both the strength of the donor-acceptor electronic coupling and the medium dynamics through  $\tau_X$ . For ions in water,  $\tau_X \simeq 0.2$  ps is close to the time of longitudinal relaxation of the polar medium.<sup>26</sup>, The Stokes-shift dynamics are much slower in proteins, 31,32 ranging from subnanosecond time scales reported by simulations of small proteins<sup>32,33</sup> to much longer relaxation times for membrane-bound protein complexes.34 This observation alone suggests that solvent-controlled electron transfer must be more ubiquitous in proteins. Electrochemical measurements<sup>35-39</sup> of half redox reactions of proteins immobilized to electrodes through self-assembled monolayers with varying thickness have shown  $R^* \simeq 15-16$  Å. This surprisingly large distance exceeds the range ~14 Å within which activated electron transfer occurs in biological energy chains assuming a millisecond reaction time and a generic value for the reorganization energy  $\simeq 0.8$  eV.<sup>40–42</sup> This reaction radius can be extended to ~25 Å for activationless transitions for electrons tunneling within a millisecond. If the electrochemical value of R\* could be applied to activated intraprotein electron transfer, that would imply that all electron-transfer hops within the protein core occur in the dynamics-controlled plateau region independent of the donor-acceptor distance. If this is confirmed, the rate of intraprotein electron transfer becomes mostly unaffected by electronic coupling (see discussion below). In this scenario, the design principle of charge-transfer chains should emphasize pushing the cofactors to the crossover distance R\* since shorter distances do not provide any rate acceleration.

Can the crossover distance  $R^*$  from interfacial electrochemistry be directly applied to intraprotein electron transfer? The issues involved are complex because the Stokes-shift dynamics alone are not sufficient to explain the values of  $R^*$  required to fit experimental rate constants. Very high values of the Stokes-shift relaxation time  $\tau_X \simeq 200$  ns, far exceeding all estimates from experiments and computer simulations, were required to fit experimental data from thin-film protein electrochemistry to the standard model of dynamics-controlled

electron transfer. 43 The resolution of this puzzle came from combining the Stokes-shift dynamics with the dynamics of protein displacements in a soft binding potential at the surface of the electrode. 28,39 Damped oscillations of the protein at the binding site modulate the electronic coupling through its exponential dependence on the distance to the electrode (eq 5) producing an additional relaxation time scale  $\tau_{\gamma} = (\gamma^2 D_R)^{-1}$ equal to the time of diffusional motion, with the translational diffusion constant  $D_R$ , through the distance of tunneling decay  $\gamma^{-1}$ . A dynamical model<sup>28</sup> combining fluctuations of the energy gap X with fluctuations of the distance to the electrode R accounts for experimental observations and allows one to reproduce large values of R\* reported experimentally. 35-39 This is achieved by requiring a sufficiently soft binding potential, effectively combining translational displacements with rotational tumbling of the protein at the binding site.<sup>3</sup> Such structural softness is unlikely to extend to donoracceptor pairs in the protein core. Nevertheless, the application of relaxation times and reorganization parameters for Trp-Cu electron transfer from the present MD simulations to the dynamical model of intraprotein electron transfer<sup>29</sup> leads to R\*  $\simeq$  12 Å (Figure 4). Even for a small globular protein, such as azurin, intraprotein electron transfer is mostly dynamicscontrolled within the range of allowed distances  $^{40,41} \simeq 14 \text{ Å}$ and is not determined by electronic coupling.

#### THEORY

**Activation Barrier.** The Gaussian statistics of the reaction coordinate X necessitates four statistical parameters: two average energy gaps  $X_i$  and two variances  $\sigma_{X,i}^2$  (eq 4). Because many particles of the medium participate in fluctuations driving the system over the activation barrier, the variances are expected to follow the macroscopic fluctuation—dissipation theorem (Johnson-Nyquist noise 4-4). It requires the variance to scale linearly with temperature allowing us to define two separate variance reorganization energies for two electron-transfer states

$$\lambda_i = \frac{1}{2}\beta\sigma_{X,i}^2 \tag{8}$$

In addition, the difference between the average energy gaps specifies the Stokes-shift reorganization energy<sup>4,5</sup>

$$2\lambda^{\text{St}} = X_1 - X_2 > 0 \tag{9}$$

In Marcus theory, all three reorganization energies are equal,  $\lambda^{\rm St} = \lambda_1 = \lambda_2$ , which we will call the Marcus limit in our calculations. This equality is not true anymore when the donor and acceptor are in different wetting environments in two electron-transfer states, as is found in our simulations described below (Figure 3). The Q-model of electron transfer 22 allows different reorganization energies as defined by eqs 8 and 9 arranged according to the following inequality

$$\lambda_2 < \lambda^{\text{St}} < \lambda_1 \tag{10}$$

In the present context,  $\lambda_1$  corresponds to the reduced state of azurin's active site, but states 1 and 2 can always be defined to satisfy eq 10. Simulations show that three reorganization energies from eqs 8 and 9 calculated from MD simulations satisfy eq 10, which allows us to apply the Q-model to modeling the energetics of electron transfer.

The free energy surfaces are nonparabolic in the Q-model

$$F_{1}(X) = (\sqrt{|\alpha||X - X_{0}|} - \sqrt{\alpha^{2}\lambda_{1}})^{2}$$

$$F_{2}(X) = \Delta F_{0} + (\sqrt{|1 + \alpha||X - X_{0}|} - \sqrt{(1 + \alpha)^{2}\lambda_{2}})^{2}$$

The parameter  $X_0$  is related to the reaction free energy  $\Delta F_0$  through the following equation

$$X_0 = \Delta F_0 - \lambda_1 \frac{\alpha^2}{1+\alpha} \tag{12}$$

The model operates with four parameters  $\lambda_1$ ,  $\lambda_2$ ,  $\lambda^{\text{St}}$ , and  $\Delta F_0$  in eq. 11. However, because of the mutual relations between them, only three parameters are independent, in contrast to two parameters,  $\lambda$  and  $\Delta F_0$ , in Marcus theory. The expressions given in eq. 11 specify two free energy surfaces in terms of two reorganization energies  $\lambda_i$  and the reaction free energy  $\Delta F_0$ . The nonparabolicity parameter  $\alpha$ , restricted by conditions  $\alpha > 0$  or  $\alpha < -1$ , is given by

$$\alpha = \frac{2\lambda^{\text{St}} + \lambda_2}{\lambda_1 - \lambda_2} \tag{13}$$

In the Marcus limit of equal reorganization energies,  $\lambda_1 \to \lambda_2$ , one obtains  $\alpha \to \infty$  and  $F_i(X)$  in eq 11 recover the limit of Marcus equal-curvature parabolas.

The first,  $X_i$ , and second,  $\lambda_i$  (eq 8), moments of the energy-gap trajectory X(t) are directly accessible from MD simulations (see SI for details). However, from the practical perspective of performing simulations of electron transfer, the second moments of the energy gap (eq 8) are often poorly converged and require extensive sampling. The first moments  $X_i$  converge much faster and offer a more convenient route to the energetic parameters of electron-transfer reactions. Since three parameters are required to fully define  $F_i(X)$  in the Q-model, one can base calculations on  $X_i$  and  $\Delta F_0$ . The reaction free energy is related to the mean of two  $X_i$  values,  $X_m = (X_1 + X_2)/2$ , as follows<sup>22</sup>

$$\Delta F_0 = X_m - \frac{\alpha \lambda_1}{2(1+\alpha)^2} \tag{14}$$

One can, therefore, calculate the nonparabolicity parameter  $\alpha$  from the average energy gaps and the reaction free energy

$$\alpha = \frac{\lambda^{\text{St}}}{2(X_m - \Delta F_0)} - \frac{1}{2} \tag{15}$$

In the Marcus model,  $\Delta F_0 = X_m$  and  $\alpha \to \infty$  when approaching the Marcus limit  $\lambda_1 \to \lambda_2$ .

Once  $X_i$  and  $\alpha$  have been established, the Stokes-shift reorganization energy follows from eq 9 and the variance reorganization energies can be calculated from the following relations in terms of  $\lambda^{\rm St}$  and  $\alpha$ 

$$\lambda_1 = \frac{2(1+\alpha)^2}{\alpha(1+2\alpha)} \lambda^{St},$$

$$\lambda_2 = \frac{2\alpha^2}{(1+\alpha)(1+2\alpha)} \lambda^{St}$$
(16)

The consistency of calculations can be checked from the requirement that  $\lambda_1$ ,  $\lambda_2$ , and  $\alpha$  satisfy the following identity

$$\zeta = \frac{\lambda_1 \alpha^3}{\lambda_2 (1+\alpha)^3} = 1 \tag{17}$$

Similarly to all previous relations, one gets all three reorganization energies equal to each other at  $\alpha \to \infty$  corresponding to the Marcus limit of the Q-model.

The disadvantage of using eq 15 as a route to the nonparabolicity parameter  $\alpha$  in the framework of MD simulations is that both  $X_m$  and  $\Delta F_0$  contain a usually unknown gas-phase energy gap. Only the Coulomb component of the energy gap is commonly calculated from simulations, supplemented in some calculations by the component from induction interactions with induced medium dipoles.<sup>45</sup> The gas-phase component of the energy gap is canceled in the difference of  $X_m$  and  $\Delta F_0$  in the denominator of eq 15 and in principle should not affect the results of calculations. However, one often wants to combine the empirical value of the reaction free energy, which contains the gas-phase component, with the statistics of the energy gap from MD simulations when the vacuum energy gap is an unknown additive component. This approach was implemented in the modeling of electrontransfer free energy surfaces as explained in more detail below.

Alternative definitions of the nonparabolicity parameter  $\alpha$  from two relations in eq 16 allow some flexibility in choosing the best converged route. The Stokes-shift reorganization energy is usually best converged since it requires first statistical moments of the energy gap (eq 9). One can therefore choose one of variance reorganization energies  $\lambda_i$  in eq 8, best converged in a given simulation, to supplement  $\lambda^{\rm St}$  and empirical  $\Delta F_0$  value to arrive at the required three parameters to fully define the Q-model. Once a given  $\lambda_i$  is chosen, one of eqs 16 is applied as the route to calculate  $\alpha$  from  $\lambda_i$  and  $\lambda^{\rm St}$ . Alternatively, one can use two  $\lambda_i$  and  $\lambda^{\rm St}$  in eq 13 to arrive at the parameter  $\alpha$ . Getting closer to satisfying the consistency condition  $\zeta = 1$  (eq 17) is the criterion for adopting a given route. The flowchart of calculations is shown in Figure 5.

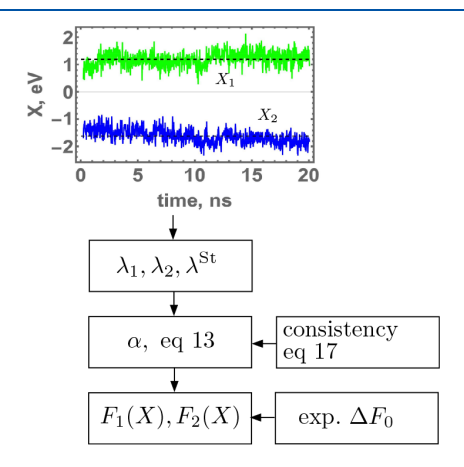
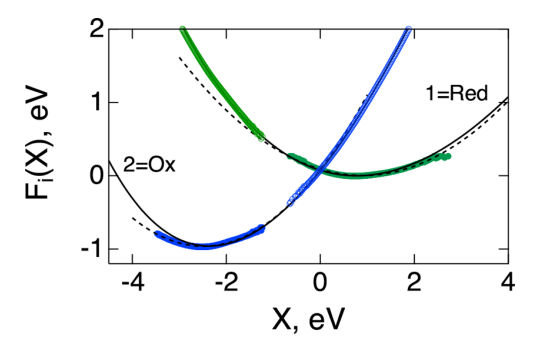


Figure 5. Flowchart of applying MD simulations to define parameters of the Q-model and construct free energy surfaces of electron transfer.

For the system studied here, alternative routes based on different values of  $\lambda_i$  yield essentially identical results for the activation barrier. Figure 6 shows  $F_i(X)$  calculated according to eq 11 with the experimental value of  $\Delta F_0 = -0.959$  eV. The MD results often do not discriminate between different models of free energy surfaces because sampling at the wings of the



**Figure 6.** Free energy surfaces of electron transfer calculated in the Q-model (eqs 11 and 12, solid lines) and compared to MD simulations (points). The calculations are based  $\lambda_i$  and  $\lambda^{\rm St}$  from MD simulations to produce  $\alpha=4.83$  according to eq 13 and the experimental value of the reaction free energy  $\Delta F_0=-0.959$  eV. The dashed lines are fits of MD data to parabolas with unequal curvatures. The upper portions of the simulation data are obtained from the results around the minima by applying the linear relation from eq 18.

distribution is insufficient and umbrella sampling is required. <sup>46</sup> Parabolas with different curvatures might seem to yield a better fit of the data (dashed lines in Figure 6), but there is no reason to assume  $\lambda_1 \neq \lambda_2$  within the standard picture of crossing parabolas even when nonergodic sampling producing  $\lambda^{\text{St}} < \lambda$  is assumed (see below).

Fits of simulation data with unequal curvature parabolas violate the linear relation between the free energy surfaces  $^{46-48}$ 

$$F_2(X) = F_1(X) + X \tag{18}$$

required when Gibbsian ensemble statistics hold. This equation follows from the straightforward manipulation of the Gibbsian statistical average for the system Hamiltonian  $H_i = E_i(q) + H_{s}$ , where the medium Hamiltonian  $H_s$  is not affected by electronic transitions

$$e^{-\beta F_1(X)} = \int dq \delta(X - \Delta E(q)) e^{-\beta H_1}$$

$$= \int dq \delta(X - \Delta E(q)) e^{\beta X} e^{-\beta H_2}$$

$$= e^{\beta X - \beta F_2(X)}$$
(19)

Equation 18 requires equality of the second derivatives of  $F_i(X)$  at each value of the reaction coordinate:  $F_1''(X) = F_2''(X)$ . This equality immediately implies that curvatures of parabolic free energy surfaces must be equal. To obtain different curvatures at the corresponding minima of  $F_i(X)$ , these functions must be nonparabolic. Such a solution is provided by the Q-model.

The Q-model, like the standard Marcus formulation, is based on Gibbsian statistics, and it satisfies the linear constraint in eq 18 (one needs to take the full solution of the model<sup>22</sup> to prove that, in contrast to the asymptotic expansion shown eq 11). Therefore, the results of simulations which sample configurations near the minima can be linearly shifted to produce far from equilibrium wings of the free-energy surfaces. This linear shift is applied to the simulation data near the minima in Figure 6 to produce the upper parts of  $F_i(X)$ . We find that the shifted data points fall on the curves produced by the Q-model (upper sets of points in Figure 6). This test allows us to discriminate between the statistically consistent Q-model from the fits to parabolas with unequal

curvatures (dashed lines in Figure 6) inconsistent with the linear constraint in eq 18.

**Pre-exponential Factor.** As discussed above, the standard formalism of the medium-controlled electron transfer assumes that overdamped medium dynamics compete with the time of electron tunneling  $\tau_e \sim \hbar/V$  in the crossing region  $F_1(0) = F_2(0)$ . The result is a crossover from a distant-dependent rate constant at large separations to a plateau region at shorter distances (Figure 4). The transition to a plateau is controlled by the crossover parameter g in the expression

$$k_{\rm ET} = (1+g)^{-1} k_{\rm NA} \tag{20}$$

where  $k_{NA}$  is given by eq 6.

The expression for the parameter g gets more complex when two-dimensional overdamped (diffusional) dynamics are considered. The activated state X=0 is still reached by diffusion in the parabolic free energy surface along the reaction coordinate X. The golden-rule expression defines the rate constant in the tunneling configuration

$$k(R) = \frac{2\pi V(R)^2}{\hbar} \delta(X)$$
 (21)

where  $\delta(X)$  is the delta-function imposing the condition of energy conservation in a radiationless transition. Diffusional reaction dynamics are accompanied by dynamical fluctuations of the donor—acceptor distance R in a harmonic potential specified by either a force constant or the variance of the donor—acceptor distance  $\sigma_{R,i}^2 = \langle (\delta R)^2 \rangle_{ii} \ \delta R = R - R_e$ . The time autocorrelation function of R(t),  $C_R^{(i)}(t) = \langle \delta R(t) \ \delta R(0) \rangle_i$  provides the integral relaxation time  $\tau_R^{(i)}$  for the distance dynamics

$$\tau_R^{(i)} = \int_0^\infty dt C_R^{(i)}(t) / C_R^{(i)}(0)$$
(22)

where i=1,2 identifies the electron-transfer state in which the dynamics are propagated.  $\tau_R^{(i)}$  can be alternatively connected to the diffusion constant  $D_R$  as  $\tau_R^{(i)} = \langle (\delta R)^2 \rangle_i / D_R$ .

The modulation of V(R) in eq 21 leads to the crossover parameter g depending on two time-scales,  $\tau_R$  for the distance dynamics and  $\tau_X$  for the Stokes-shift dynamics. The resulting expression is  $^{29}$ 

$$g = \frac{2\pi V_e^2 \tau_X}{\hbar \sigma_X} \frac{e^{3\gamma^2 \langle (\delta R)^2 \rangle / 2}}{\sqrt{2\beta \Delta F^{\dagger} + 4(\tau_X/\tau_R) \gamma^2 \langle (\delta R)^2 \rangle}}$$
(23)

where here and below we drop the dependence on the charge-transfer state i=1,2 for brevity. Further,  $V_e$  is the electronic coupling at the equilibrium donor—acceptor distance in eq 5 and  $\Delta F^{\dagger}$  is the activation barrier specified by the vertical distance from the free-energy minimum to the crossing point at X=0 (Figure 6). The effective relaxation time entering the parameter g is scaled with the factor  $\exp[(3/2)\gamma^2((\delta R)^2)]$ . This implies that softer proteins, with shallower potentials of mean force for altering the donor—acceptor distance, will produce slower effective relaxation times affecting the crossover behavior. Such nonrigid media must have a greater propensity to fall into the plateau regime for the rate constant controlled by the medium dynamics (Figure 4).

**Protein Scaffold.** The non-Gaussian Q-model allows nonequal reorganization energies as specified by eq 10 through the mechanism of electrowetting of the Trp residue. A mechanism more common for proteins to lower the activation

barrier is through nonergodic sampling of configuration space by the protein. We first review mechanistic consequences of nonergodic sampling for the reaction activation barrier and then investigate the possibility of yet another alternative mechanism for separating the reorganization energies related to changing the protein stationary polarization in two oxidation states.

Both the standard Marcus formulation <sup>11</sup> and the Q-model <sup>22</sup> are theories based on the Gibbsian prescription for producing statistical weights for system configurations: the linear relation in eq 18 is limited to this framework. If some parts of configuration space are restricted, either by geometrical constraints of the protein fold or through dynamical restrictions requiring times too long to reach them, statistical weights of configurations do not strictly follow the Gibbsian recipe based on the ergodic assumption that all essential states are sampled on the time of observation. <sup>50</sup> The change of statistical rules leads to the breakdown of the link between the first and second moments of the reaction coordinate *X* (eqs 8 and 9) stipulated by the fluctuation—dissipation theorem. <sup>51</sup> Phenomenologically, this breakdown is expressed by the inequality

$$\lambda^{\text{St}} < \lambda$$
 (24)

replacing the corresponding equality in Marcus theory. 49 Such nonergodic effects on the electron-transfer kinetics are most pronounced for large, often membrane-bound, protein complexes, 17,34,52 where the protein is the main component of the thermal bath affecting the activation barrier. For instance, a long,  $\sim 15 \mu s$ , MD simulation of the bc<sub>1</sub> complex<sup>49</sup> has shown that opening longer observation windows from the simulation trajectory makes the variance reorganization energy (eq 8) increase without saturation through the entire simulation time. However, statistical convergence, not reachable for a large protein complex, is attained on the simulation time of 200-300 ns for small globular proteins, such as azurin considered here. Despite this convergence, the protein component of the thermal bath shows a strong separation between  $\lambda^{\text{St}}$  and  $\lambda$  according to eq 24, suggesting that the jammed and frustrated protein interior promotes glassy dynamics<sup>53</sup> with strong features of nonergodic sampling.<sup>5</sup> It is currently not clear if this is just the size of the protein complex or the membrane that acts to dehydrate a part of the protein to allow eq 24 for large membrane-bound protein complexes. However, dehydration provides a natural control mechanism of protein's activity: a small globular protein becomes redox-active when binding to a large protein complex partially eliminates its hydration shell.

A potential mechanism for separating the Stokes-shift and variance reorganization energies, distinct from nonergodic sampling, is related to the stationary polarization of the protein interior by the electric field of ionized surface residues. Polarization models of electron transfer dientify the harmonic spring coordinate in Figure 2 with the nuclear (slow) polarization of the medium P. The interaction of the transferring electron with the medium includes its interaction with the polarization  $\mathbf{P}_0$  in equilibrium with the charges of the donor—acceptor complex and the interaction with the thermally induced fluctuation  $\delta \mathbf{P}$ . The latter can be identified as the displacement coordinate q in Figure 2. The electric field of the electron changes with electronic transition yielding the difference of electric fields  $\delta \mathbf{E}_e$  from the electron in two states. Its interaction with  $\delta \mathbf{P}$  makes the fluctuating part of the

reaction coordinate X, while the interaction of  $\Delta \mathbf{E}_e$  with  $\mathbf{P}_0$  contributes to the equilibrium energy gap  $X_i$  in each state.

The Marcus formulation assumes that the equilibrium polarization  $\mathbf{P}_0$  is caused by the donor—acceptor complex, i.e., bulk polar liquid considered in the theory is not polarized. Therefore, one assigns the polarization  $\mathbf{P}_0 = \mathbf{P}_1$ , induced by the electric field of the donor—acceptor complex, to the initial charge-transfer state. Standard arguments of linear solvation theories then allow one to write  $X_1$  as a sum of the reaction free energy and the standard Marcus reorganization energy  $\Delta F_0 + \lambda$ . This is the vertical energy gap  $X_1$  for the forward electronic transition in Marcus theory; the same arguments produce  $\Delta F_0 - \lambda$  for the backward transition. What is not anticipated in the Marcus formulation is the possibility of a stationary polarization of the medium  $\mathbf{P}_0$  unrelated to electrostatics of the donor—acceptor complex. In other words, the medium is paraelectric, but not ferroelectric.

A nonzero stationary polarization in the molecule's body frame is, however, always present in the protein interior given that strong internal electric fields have been reported for proteins due to ionized surface residues. <sup>57</sup> Such a stationary medium polarization does not typically cause difficulties since it creates a constant shift of  $X_i$  and cancels out in the Stokes shift in eq 9. However, structural changes of the protein might cause different polarization fields in two oxidation states (Figure 7), which do not cancel in the difference. One

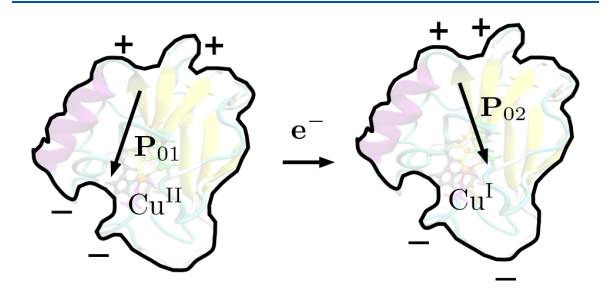


**Figure 7.** Schematic drawing of the half reaction of azurin altering the internal polarization of the protein scaffold.

therefore gets  $\mathbf{P}_{01}$  in the initial state and  $\mathbf{P}_{02}$  in the final state. The resulting Stokes shift becomes

$$2\lambda^{\text{St}} = X_1 - X_2 = 2\lambda - \int_{\Omega_p} d\mathbf{r} \Delta \mathbf{P}_0 \cdot \Delta \mathbf{E}_e$$
(25)

where  $\Delta P_0 = P_{02} - P_{01}$ , and integration is performed over the protein volume  $\Omega_p$  excluding the donor and acceptor.

What is significant is that the change in the polarization  $\Delta P_0$ , even though triggered by electron transfer, is not related in any straightforward way to the electrostatic field of the electron. The corresponding local basin of protein stability becomes unstable as a result of electron transfer and the protein transforms to a new conformation dictated by its internal structural motifs and not by electron's electrostatics. In this regard, the change of the global polarization of the protein is a nonlinear transformation: it cannot be related by a linear relation, through a susceptibility function, to either electron's electrostatic potential or field.

Assuming the uniform polarization  $P_0$ , the second term in eq 25 can be written as

$$-\int_{\Omega_p} d\mathbf{r} \Delta \mathbf{P}_0 \cdot \Delta \mathbf{E}_e \simeq -\Delta \mathbf{M}_0 \cdot \langle \Delta \mathbf{E}_e \rangle_{\Omega}$$
(26)

where  $\Delta \mathbf{M}_0$  is the difference of dipole moments of the protein calculated from molecular charges excluding the charges of the donor and acceptor. Further, the vector  $\Delta \mathbf{E}_e$  is averaged over the protein volume  $\Omega_p$  excluding the volumes of the donor and acceptor

$$\langle \Delta \mathbf{E}_{e} \rangle_{\Omega} = \frac{1}{\Omega_{p}} \int_{\Omega_{p}} d\mathbf{r} \Delta \mathbf{E}_{e}$$
(27)

Approximating  $\Delta \mathbf{E}_e$  with the field produced by the electron transfer dipole  $\boldsymbol{\mu}_{\rm ET}$  (pointing from the negative acceptor to the positive donor), one obtains

$$\langle \Delta \mathbf{E}_e \rangle_{\Omega} \propto \boldsymbol{\mu}_{\mathrm{ET}}$$
 (28)

From eqs 25, 26, and 28, the Stokes-shift reorganization energy is modified compared to  $\lambda$ 

$$2\lambda^{\text{St}} = 2\lambda - A\boldsymbol{\mu}_{\text{ET}} \cdot \Delta \mathbf{M}_0 \tag{29}$$

where A is a constant incorporating specifics of the protein and charge-transfer geometry (see below). The main result of these arguments is that one can obtain either inequality 24 or  $\lambda^{\rm St} > \lambda$  depending on the sign of the second term in eq 29. Either scenario does not require nonergodic sampling and thus can be fully formulated within the Gibbsian framework. The linear relation in eq 18 must be satisfied, and it provides a reliable test for applying this nonlinear mechanism.

#### **■ RESULTS OF SIMULATIONS**

**Reorganization Parameters.** The reaction studied by Shih et al.  $^6$  consists of transferring a hole, induced by photoexcited Re<sup>I</sup>-diimine attached to the surface of azurin, from the Trp $^+$  cation radical to Cu<sup>I</sup>

$$(1)Cu^{I} - Trp^{+} \xrightarrow{k_{ET}} Cu^{II} - Trp(2)$$
(30)

Here, 1 and 2 mark the initial and final states, respectively. Correspondingly, the reaction coordinate is defined as the difference of energies in the final and initial states, for which only the Coulomb part  $X^{C}$  is calculated from MD trajectories

$$X^{C} = \sum_{i \in D} \Delta q_{i}^{D} \phi_{i}^{D} + \sum_{i \in A} \Delta q_{i}^{A} \phi_{i}^{A}$$

$$(31)$$

The unknown offset due to nonelectrostatic components of the energy gap is evaluated by horizontally shifting the free energy surfaces  $F_i(X)$  to make them cross at X = 0 (Figure 6).

The simulation trajectories were produced as described elsewhere<sup>54</sup> and in more detail in the SI. Briefly, the X-ray diffraction structure of *Pseudomonas aeruginosa* azurin (resolution 2.70 Å, PDB 1AZU<sup>58</sup>) was adopted as the starting configuration for MD simulations. The Red and Ox states of azurin were created as described elsewhere.<sup>54</sup> Trp was modified to the oxidized form with atomic charges either adopted from the literature<sup>59</sup> or calculated here using CDFT protocol with the 6-31+G\* basis set (Tables S1 and S2). The wetting pattern of Trp+ changes between two charge distributions (Figure S14), although the qualitative picture stays the same. MD simulations with 36469 TIP3P water molecules in a cubic simulation box were performed with NAMD<sup>60</sup> applying the 2 fs time step and particle mesh Ewald for electrostatic interactions. The length of production NVT trajectories for all states was 300 ns.

The variance (eq 8) and Stokes-shift (eq 9) reorganization energies for the reaction shown in eq 30 are listed in Table 1.

Table 1. Reorganization Energies (eV) for the Entire System (Azurin and Hydration Water) and for the Protein and Water Components Separately from MD Simulations at  $T=300~\rm K$ 

	protein+ water		protein		water	
State	λ	$\lambda^{\mathrm{St}}$	λ	$\lambda^{\mathrm{St}}$	λ	$\lambda^{\mathrm{St}}$
Trp+-CuI	2.09	1.65	2.39	0.82	3.57	0.83
Trp-Cu <sup>II</sup>	1.17		1.28		1.25	

The Stokes-shift reorganization energy falls between two variance reorganization energies as required by eq 10 specific to the Q-model. The nonparabolicity parameter  $\alpha=4.83$  is found from eq 13 (Figure 5). The consistency of the model is tested by calculating the parameter  $\zeta\simeq0.98$  in eq 17. The free energy surfaces shown in Figure 6 are plotted based on eqs 11 and 12 to which the variance reorganization energies from simulations  $\lambda_i$  are substituted along with the nonparabolicity parameter  $\alpha=4.83$  and experimental reaction free energy  $\Delta F_0$ .

The reorganization parameters for the protein component of the thermal bath also show a strong separation between the Stokes-shift and variance reorganization energies according to eq 24, but also  $\lambda_1 \neq \lambda_2$  due to different wetting states of the oxidized and reduced Trp (Figure 3). We find  $\lambda^{\text{St}} < \lambda_i$  for the protein component (Table 1), making the Q-model inapplicable in this case (compare to eq 10). It is also worth noting that the variance reorganization energies from the protein component are close in magnitude to the corresponding total reorganization energies. This does not mean that the water component of the reorganization energy is small. The total reorganization energy is not a simple addition of the protein and water components because of a cross-correlation between the protein and water terms in the variance of the energy gap in eq 8. The cross-correlation contributes a negative term, often exceeding in magnitude individual self-terms (Table 1), to the variance reorganization energy.

**Stokes-Shift and Distance Dynamics.** The Stokes-shift dynamics were monitored by the Stokes-shift time correlation function

$$C_X^{(i)}(t) = \langle \delta X(t) \, \delta X(0) \rangle_i \tag{32}$$

where the dynamics of the energy gap coordinate X(t) is produced from the MD trajectory by calculating the Coulomb interaction energy of the donor and acceptor with the protein—water thermal bath according to eq 31. The dynamics can be propagated in either of two charge-transfer states in eq 30, which is specified by the subscript in the average  $\langle \cdots \rangle_i$ . The results are shown in Figure 8 for two charge-transfer states and are compared to the Stokes-shift dynamics for the electrochemical half reaction of azurin reduction. <sup>54</sup> The characteristic relaxation times  $\tau_X^{(i)}$  obtained from multiexponential fits (SI) are in the range of  $\sim 20-116$  ps depending on the state considered (Table 2).

The relaxation times of the Stokes-shift dynamics found here are not necessarily representative of all proteins:  $\tau_X \sim 1$  ns was found for the oxidized form of cytochrome and  $\tau_X \sim 395$  ns for electron transfer between the quinol substrate and the Fe<sub>2</sub>S<sub>2</sub> active site of the Rieske protein in the bacterial bc<sub>1</sub> complex. Note that the Stokes-shift dynamics reported by

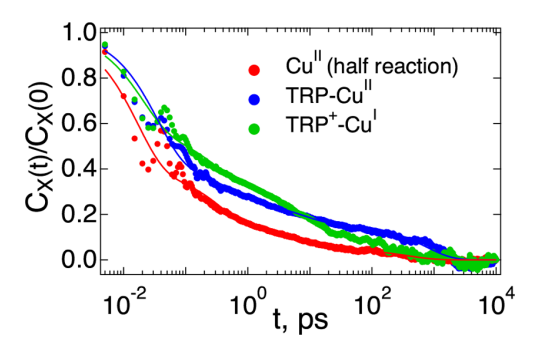


**Figure 8.** Normalized Stokes-shift time autocorrelation function (eq 32) for two states of charge transfer (eq 30) and for the half reaction of azurin reduction (Cu<sup>II</sup> half reaction). Points are results of MD simulations and solid lines are fits to multiexponential functions (see SI).

Table 2. Relaxation Times (ps) and Donor-Acceptor Distance for Cu-Trp Charge Transfer (eq 30). Also Listed Is the Crossover Parameter g from eq 23 and the Rate Constants  $k_{\rm NA}$  (eq 6) and  $k_{\rm ET}$  (eq 7)

State	$\tau_X^{\ a}$	$ au_R$	⟨ <i>R</i> ⟩, Å	$\langle (\delta_{\mathring{A}}^{R})^{2} \rangle$ ,	g	$k_{ m NA}$ ns $^{-1}$	$k_{\rm ET}$ , ns <sup>-1</sup>
Trp+-CuI	44	19	10.3	0.52	31	11	0.34
Trp-Cu <sup>II</sup>	116	17	9.2	0.12	50		

 $^a au_{\chi}$  for the half reaction of azurin reduction is 19.4 ps (see Figure S4 and Table S3).

chromophores attached to the protein surface<sup>32</sup> do not necessarily reflect the dynamics of fluctuations driving intraprotein electron transfer or a half redox reaction.

The dynamics of the donor-acceptor distance R(t) were monitored by the distance time autocorrelation functions calculated from MD trajectories (Figure 9)

$$C_R^{(i)}(t) = \langle \delta R(t) \, \delta R(0) \rangle_i \tag{33}$$

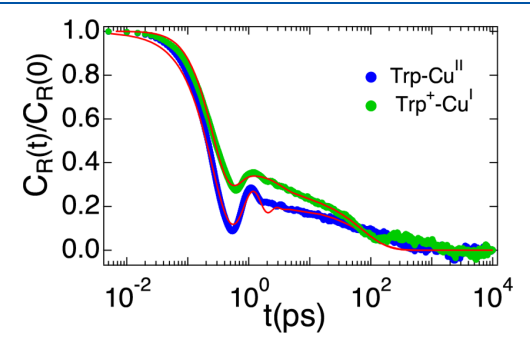


**Figure 9.** Normalized time autocorrelation function for the donor–acceptor distance (eq 33). Points are results of MD simulations in two electron-transfer states and red solid lines are fits to analytical functions explained in the SI.

The average donor—acceptor distance  $\langle R \rangle_{\nu}$  distance variance  $\langle (\delta R)^2 \rangle_{\nu}$  and the integral relaxation times (integral of the normalized time correlation function)  $\tau_R^{(i)}$  are listed in Table 2. The distribution of distances is approximately Gaussian for the final charge-transfer state i=2, but it has two maxima corresponding to two equilibrium positions of the positively charged indole ring of Trp in the initial charge-transfer state i=1

1 (Figure S16). This is the reason for a more substantial distance variance in that state (Table 2).

Internal Protein Polarization. Changing internal protein polarization can produce inequality between the Stokes-shift and variance reorganization energies (eq 29). This possibility was studied by calculating trajectories of the dipole moment  $\mathbf{M}_0 = \sum_j q_j \mathbf{r}_j$  from azurin charges excluding the charges of the donor and acceptor sites (Trp and Cu active site); the coordinates  $\mathbf{r}_j$  of partial charges  $q_j$  are taken relative to the protein center of mass. We found a significant change in the magnitude of the dipole moment from  $M_{01} \simeq 104$  D in the initial state to  $M_{02} \simeq 82$  D in the final charge-transfer state. Sampling of the cosine between  $\mathbf{M}_{0i}$  and the electron transfer dipole  $\boldsymbol{\mu}_{\mathrm{ET}} = -e\mathbf{R}$  shows that  $\mathbf{M}_{0i}$  and  $\boldsymbol{\mu}_{\mathrm{ET}}$  align with the angle  $<90^{\circ}$  (Figure 10) and, therefore, potential rotation of the

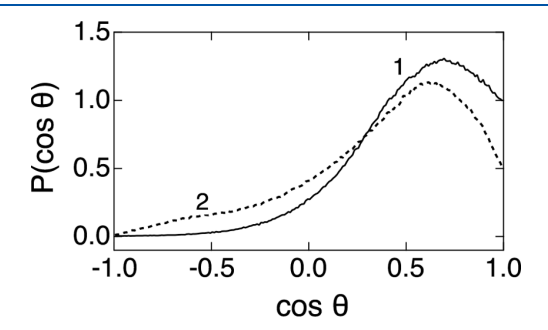


**Figure 10.** Distribution of cosines  $\cos \theta \propto \mu_{\rm ET} \cdot \mathbf{M}_{0i}$  for the initial (i = 1, eq 30) and final (i = 2, eq 30) charge-transfer states. The dipole moment  $\mathbf{M}_{0i}$  is calculated relative to the center of mass of azurin from atomic charges excluding the charges of Trp and the active site.

protein dipole does not contribute to the sign of the second terms in eq 29. On the other hand, the value of the dipole moment does change. Given  $\Delta M_0 \simeq -22$  D, the sign of the second term in eq 29 is determined by whether the average field  $\langle \Delta E_e \rangle_{\Omega}$  is parallel or antiparallel to  $\mu_{\rm ET}$ .

The direction and position of the electron-transfer dipole within the protein determine whether the average electric field of the electron-transfer dipole  $\langle \Delta \mathbf{E}_e \rangle_{\Omega}$  is along  $\boldsymbol{\mu}_{\rm ET}$  (parallel) or opposite to  $\boldsymbol{\mu}_{\rm ET}$  (antiparallel). Two possible configurations are sketched in Figure 11. The field of a dipole averages out to

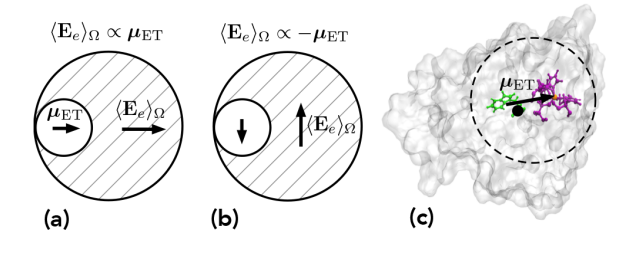


Figure 11. Schematic drawing of orientations of the electron-transfer dipole  $\mu_{\rm ET}$  relative to the geometrical center of the protein. The open sphere indicates the region where the electric field of the electron-transfer dipole averages out to zero. The shaded region indicates the part of the protein volume that contributes to  $\langle \Delta E_e \rangle_{\Omega}$ . (a) and (b) indicate configurations when the average electric field is either parallel or antiparallel to the electron-transfer dipole; (c) shows the electron-transfer dipole in azurin. The black dot is the protein's center of mass. The dashed circle refers to an approximate region where the field of the electron-transfer dipole averages to zero.

zero within a spherical volume. Therefore, the average field  $\langle \Delta E_e \rangle_\Omega$  is determined by its direction within the volume outside of a sphere drawn around the electron-transfer dipole with the radius equal to the closest distance to the solvent. Depending on the orientation of  $\mu_{\rm ET}$  relative to the asymmetric part of the protein volume, one finds the average field either parallel (Figure 11a) or antiparallel (Figure 11b) to  $\mu_{\rm ET}$ . Which of the two scenarios applies to azurin is hard to decide because of its complex shape (Figure 11c). From the protein geometry, the average electric field  $\langle \Delta E_e \rangle_\Omega$  should be nonzero, but whether the second term in eq 29 is negative remains unclear.

Given a strong separation between the Stokes-shift and variance reorganization energies for the protein component (Table 1), one wonders which mechanism, nonergodic sampling or altering internal protein polarization, is the origin. The linear relation between the free energy surfaces (eq 18) can provide a clue here. If a currently unknown Gibbsian statistical model can be constructed to reproduce the observed phenomenology, the corresponding free energy surfaces should satisfy the linear relation in eq 18. However, the free energy surfaces for the protein component of the thermal bath (Figure 12) do not satisfy this relation suggesting that it is the

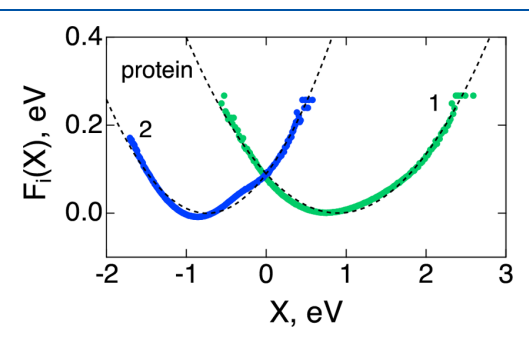


Figure 12. Free energy surfaces of electron transfer for the protein component of the thermal bath from MD simulations (points). The dashed lines are fits to parabolas with unequal curvatures. The free energy surfaces are plotted with zero reaction free energy.

nonergodic character of sampling of the protein configurations that is the reason for the separation of reorganization energies according to eq 24. Fluctuations of hydration water, coupled to protein motions, mask this physics into an overall statistical ensemble that fits well to the Gibbsian Q-model (Figure 6).

Rate Constants. The reaction of hole transfer  $1 \rightarrow 2$  (eq 30) is energetically downhill, with the reaction free energy  $\Delta F_0 = -0.959$  eV following from the reduction potentials of azurin  $^{62}E^0 = 0.341$  and  $1.3 \text{ V}^{9,63}$  for the formation of the radical cation  $\text{Trp}^+$  (from  $\simeq 0.952 \text{ V}^{64}$  to  $\simeq 1.1 \text{ V}^{63}$  for the neutral radical). For the rate constant calculation, one needs to specify distance dependence of the electronic coupling in eq 5. This function has not been calculated for the Cu-Trp pair and we used the function proposed by Voityuk and applied elsewhere for the coupling between iron—sulfur clusters:  $\log_{10}[V/\text{eV}] = 1.73 - 0.42 \times R$ , where R (Å) is the distance between the centers of the donor and acceptor. This function, which implies  $\gamma = 1.93 \text{ Å}^{-1}$  in eq 5, is numerically close to Hopfield's equation  $rac{67}{4}$  applied to the electronic coupling between Trp residues ( $\gamma \simeq 1.1 \text{ Å}^{-1}$  was reported experimentally.

The activation barrier  $\Delta F^{\dagger} = F_1(0) - F_{\min,1} \simeq 0.075$  eV in eq 7 was calculated from the Q-model as the vertical distance

between the crossing point of the free energy surfaces and the corresponding free-energy minimum  $F_{\rm min,1}$ . The calculated nonadiabatic rate constant  $k_{\rm NA}$  (eq 6) and the full electron-transfer rate constant  $k_{\rm ET}$ , incorporating the medium dynamical effect (eq 7), are listed in Table 2 for the forward reaction of Trp+ reduction in eq 30. The backward reaction is too slow because of a high negative driving force (see the free energy surfaces in Figure 6). The most dramatic deviation from standard theories is a large value of the crossover parameter  $g \simeq 31$  substantially increasing the reaction time from  $\tau_{\rm NA} = k_{\rm NA}^{-1} \simeq 91$  ps to  $\tau_{\rm ET} = k_{\rm ET}^{-1} \simeq 2.9$  ns. The reaction rate is therefore limited by the medium dynamics.

From our calculations, the second term under the square root in eq 23 for the dynamical crossover parameter substantially exceeds the first one for the forward reaction, but not for the backward transition. In the former case, the crossover parameter is given by a somewhat simplified relation

$$g \propto V_e^2 \sqrt{\tau_X \tau_R} e^{(3/2)\gamma^2 \langle (\delta R)^2 \rangle}$$
 (34)

which depends on the dynamics through the geometric mean of the relaxation times  $\tau_X$  and  $\tau_R$ . The dependence of g on the variance of the donor—acceptor distance  $\langle (\delta R)^2 \rangle$  and the corresponding distance relaxation time implies that the rate of electron transfer is affected by protein elasticity. Changes in elasticity due to protein function or substrate binding can thus affect the electron-transfer rate (allosteric effect). The time of  ${\rm Trp}^+$  reduction  $\simeq 3$  ns is below the reaction time  $\simeq 31$  ns reported experimentally. Note that putting the activation energy equal to zero brings the reaction time down to  $\simeq 200$  ps. It can be compared to  $\sim 1$  ns reported  $^{69}$  for electron transfer between photoexcited Trp and Cu<sup>II</sup> in azurin. Similarly, electron-transfer quenching of photoexcited Trp by heme of myoglobin  $(R \simeq 12 \text{ Å})$  requires  $\simeq 40 \text{ ps.}^{70}$ 

There are several sources of uncertainty contributing to  $\simeq$ 28 ns difference between the calculated and measured reaction times. In addition to uncertainty in assigning the electronic coupling to this reaction, the redox potential of Trp+ measured in ref 63 for  $\alpha_3$ W model protein, might not apply to Trp-48 residue of azurin. Applying the difference at pH = 7 between  $\alpha_3$ W (1.1 V) and Trp-48 of azurin (0.952  $V^{64}$ ) to the redox potential of the Trp cation radical, one obtains the reaction free energy  $\Delta F_0 \simeq -0.81$  eV compared to  $\Delta F_0 \simeq -0.959$  eV adopted in our calculations. This correction leads to the reaction time of  $\simeq 10$  ns. Still remaining difference between the calculated and reported reaction times might be caused by the time of wetting of Trp+ required to achieve the reaction conditions. Indeed, the Trp+ pocket, which was dry at the beginning of simulations, acquires the equilibrium number of water molecules on the time scale of  $\simeq 20$  ns (Figure S15). Deprotonation of Trp+ occurs on a much longer time scale of ~200 ns<sup>69,71</sup> and cannot compete with Trp<sup>+</sup> reduction.

#### DISCUSSION

A folded protein is a closely packed and elastically rigid structure when compared to the surrounding hydration water.<sup>72</sup> Considering it as a structured medium for carrying enzymatic reactions comes in conceptual conflict with the belief, widely held in biology, that much of nature's function has been highly optimized by evolution.<sup>73</sup> Protein electron transfer comes as a striking contradiction to this dogma as it seems there is very little room for fine-tuning the reaction rate and adjusting the activation barrier. Two components mostly

influence the rate constant: electronic coupling and the activation barrier. The distance decay of the tunneling probability does change with the intervening medium, but the range of change does not allow a highly specific catalytic function ( $\gamma$  changes from 1.55–1.65 Å<sup>-1</sup> for an aqueous glass to 1.1 Å<sup>-1</sup> for proteins<sup>68</sup>). From the side of the activation barrier, the reorganization energy of protein electron transfer is often viewed as a generic parameter,  $\sim$ 0.8 eV, characterizing essentially all electron-transfer events in biological energy chains. The only parameters remaining to tune in this picture is the reaction free energy and the tunneling distance. The main focus of bioenergetics is hence on structure and redox potentials.

If tunability of the activation barrier for redox reactions is not a part of essential properties provided by protein reaction media, does it mean that proteins do not catalyze electron transfer? This is not the case, as Gray and Winkler's pointed out long ago: the protein environment significantly lowers the activation barrier compared to reactions in solution. The barrier depression by the protein matrix also does not seem to follow Pauling's prescription anticipating that the activated complex has to be preferentially stabilized by an enzyme. 76,77 The highly successful Marcus theory of electron transfer derives the activation barrier solely from equilibrium properties of the fluctuating medium in two charge-transfer states, and no special role is given to the protein-water thermal bath at the state of the activated complex. Instead, the activated state is prescribed by the crossing of parabolas constructed from equilibrium statistics at their corresponding minima and not from configurations at the nonequilibrium transition state.

The fluid and omnipresent water appears as a natural alternative to the picture of a rigid protein unable to alter its structure to accommodate transfer of a single charge (in contrast to other reactions in which conformational changes are involved). An increasing number of examples indicate the possibility of electrowetting of protein pockets<sup>78</sup> and active sites of enzymatic reactions following charge alteration <sup>15–18</sup> and light absorption.<sup>79</sup> The present study has addressed the question of what are the generic consequences of active site wetting for the kinetics of protein charge transfer.

The main mechanistic consequence of distinct wetting patterns of electron-transfer cofactors is the ability to substantially change the force constant of nuclear fluctuations projecting on the electron-transfer reaction coordinate. We find that the Q-model addressing this phenomenology allows different variance reorganization energies. This perspective has a potential of extension to other problems where structural changes of the protein—water medium between the initial and final reaction states require considering Gaussian near-equilibrium fluctuations with different force constants.

In addition to the reorganization parameters of the entire protein—water system, we have calculated the reorganization parameters of protein alone. The protein subsystem shows a substantial separation of the Stokes-shift and variance reorganization energies that follows phenomenology of nonergodic sampling (eq 24). It anticipates that the separation between first and second moments of the reaction coordinate occurs because the average values  $X_i$  refer to local minima of the system energy landscape in which the system gets stuck, while the variances represent a broader sampling of the system fluctuations. The significance of nonergodic sampling was demonstrated for the bacterial  $bc_1$  complex where the variance reorganization energy of electron transfer kept continuously

increasing on the 15  $\mu$ s simulation trajectory when longer sampling windows were allowed.<sup>34</sup> For a much smaller azurin protein, it appears that  $\lambda$  is reasonably converged on a ~300 ns trajectory and one wonders if there are alternative mechanisms to allow the separation of the first and second moments of the reaction coordinate.

We have proposed here that the interaction of the electrontransfer dipole with the polarization of the protein interior induced by its intrinsic charge distribution can provide such a mechanism. If a structural alteration of the protein, induced by charge transfer, alters the intrinsic polarization within the protein, this alteration adds a term to the Stoke-shift reorganization energy destroying its equivalence with the variance reorganization energy (eq 25). The change of the intrinsic protein polarization is caused by structural instability and cannot be related linearly to the altering electrostatics of the donor and acceptor. This is, therefore, a nonlinear response which can trigger the observed separation between two reorganization energies. Despite some indications supporting this mechanism, we could not definitively connect it to the averages produced by MD. Moreover, the free energy surfaces of electron transfer for the protein component of the thermal bath (Figure 12) do not follow the anticipated linear relation (eq 18), suggesting nonergodic sampling. While alternative mechanisms can be sought, nonergodicity remains the leading explanation for the catalytic effect of proteins on redox reactions.

Medium dynamical control of electron-transfer kinetics gains in importance for protein electron transfer due to slower Stokes-shift dynamics compared to standard expectations for polar molecular solvents placing the relaxation time to the subpicosecond domain. In contrast, the Stokes shift relaxation time falls to the 10-100 ps window for proteins (Table 2). When controlled by the medium dynamics, the electron-transfer rate constant becomes independent of the donor—acceptor distance, and of the electronic coupling, within the separation range  $R < R^*$  determined by the condition of  $g(R^*) = 1$  (Figure 4).

We have identified a new mechanism of medium dynamics controlling the reaction kinetics by mixing the Stokes-shift dynamics due to medium's electrostatics with dynamics of the donor-acceptor distance modulating the probability of electron tunneling. The electrostatic and distance fluctuations relax on comparable time scales and thus strongly mix in the crossover parameter g (eq 23). However, a large variance of the distance between the active site and the flexible indole ring of Trp leads to a simplified equation for g (eq 34) making the geometric mean of two relaxation times the main dynamic parameter specifying the crossover to the medium dynamical control. The main result of the calculations is that reduction of Trp<sup>+</sup> is fully in the regime of dynamical control of the rate constant, which is strongly reduced, by a factor  $g \simeq 31$ , compared to the prediction for nonadiabatic electron transfer (Figure 4). Electron transport from the active site over the chain of relay elements appears to be not optimized in terms of the distance between them since the indole ring of the Trp residue could have been shifted to  $R^* \simeq 12$  Å without significant loss of the hopping rate (Figure 4). Note that our definition of the distance R is based on the distance between the centers of electron localization. It needs to be amended when compared to the edge-to-edge distance metric often applied to intraprotein electron transfer<sup>42</sup> or to the thickness of the insulating monolayer in electrochemical measurements <sup>81,82</sup> discussed next.

The conclusion that the rates of Trp<sup>+</sup> reduction and oxidation are dynamically controlled, similarly to corresponding thin-film protein electrochemistry data, seems to fall in disagreement with the distance scaling of protein electron transfer suggested by Dutton and co-workers. 40-42 Figure 13

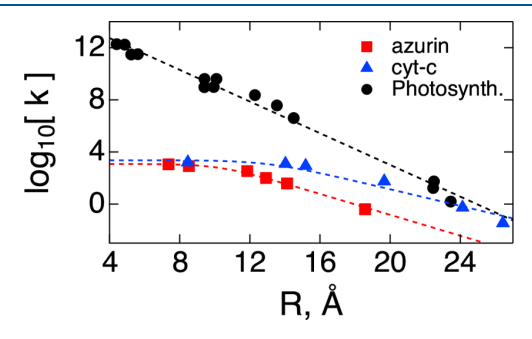


**Figure 13.** Apparent rate constants<sup>82</sup> of electron transfer between a metal electrode and different proteins immobilized on SAMs of varying thickness: azurin (red points) and cytochrome c on pyridineterminates SAMs (blue points).<sup>81</sup> The rates are plotted against the thickness of the SAM layer. These data are compared to photosynthetic rate constants plotted vs edge-to-edge distances between the redox cofactors (black points).<sup>83</sup> The dashed lines are fits through the points.

compares the rates for photosynthetic electron transfer with those reported by thin-film protein electrochemistry. 81,82 The distant scales do not have to coincide for the two sets of data since the electrochemical (apparent) rates are plotted against the thickness of the self-assembled monolayer (SAM) at the surface of the electrode and photosynthetic rates are plotted vs the edge-to-edge distance between the electron-transfer cofactors. Photosynthetic rates are corrected for the Boltzmann activation term and thus represent the rate constant preexponential factor. These data show no indication of the anticipated by theory<sup>25,26,28,29</sup> (eq 7) plateau clearly reached by electrochemistry. Instead, the rates continue an exponential distance dependence nearly to the van der Waals contact between the cofactors. The discrepancy between two sets of data and with theory expectations is puzzling and requires further studies. A possible resolution can be sought from the fact that close-contact rates of photosynthetic primary charge separation are very fast, in the domain of a few picoseconds, when dynamic nonergodicity becomes significant. 45 The slow medium modes that make the dynamical control of electron transfer possible become dynamically frozen on the fast reaction time scale. Calculations of rates require a selfconsistent solution for the reaction dynamics and nonergodic free energy surface over which diffusional dynamics proceed to the resonance tunneling configuration. 84-86 A clear signature of nonergodic dynamic freezing is the reduction 45,84 in the reorganization energy for primary charge separation from the thermodynamic limit of  $\sim$ 2.46 eV obtained by MD to the experimentally observed<sup>87</sup> value of  $\sim$ 0.35 eV.

The condition  $R > R^*$  avoiding the plateau region for electron transfer also implies that design strategies based on stacking cofactors or aromatic residues to enhance conductivity cannot be effective. Such a mechanism, in terms of conductivity through aromatic residues, has been suggested

to provide charge transport through microbial pili polymers. Recent experimental and theoretical evidence, however, suggests that these polymers are less ordered than hypothesized and have conductivities orders of magnitude lower than originally anticipated. The microbial conductivity is instead allowed by OmcS and OmcZ nanowires of cytochrome hemes stacked at 3.5–5 Å edge-to-edge distance. The role of dynamical medium control of electron transfer in these ordered stacks still needs to be understood.

#### CONCLUSIONS

In summary, we have addressed the question of whether redox activity of proteins can be tuned by the protein-water thermal bath or, alternatively, protein electron transfer is governed by universal activation and tunneling parameters making the tunneling distance and the driving force the only parameters to alter the reaction rate. A major mechanism of tuning protein electron transfer is nonergodic sampling when the activation barrier is lowered due to the separation between the Stokesshift and variance reorganization energies. This mechanism does not anticipate different variance reorganization energies in two redox states. However, this possibility is allowed by electrowetting of the active site which, in the present simulations, leads to a strong separation between two variance reorganization energies. Dynamics of the protein-water medium strongly affect the reaction rate. The rate constant is independent of the donor-acceptor distance (stays at a plateau) for  $R < R^*$ . This finding suggests that optimum operation of energy chains of biology, maximizing both the rate of electron transport and the distance traveled, is achieved by placing the electron-transfer cofactors near the crossover distance R\*. Medium dynamics controlling electron transfer allow protein elasticity and flexibility to affect electron-transfer rates. A large value of  $R^* \simeq 12$  Å found here, even though below  $R^* \simeq 15-16$  Å from thin-film protein electrochemistry, puts most intraprotein electron-transfer reactions under the umbrella of dynamical control.

#### ASSOCIATED CONTENT

#### Supporting Information

The Supporting Information is available free of charge at https://pubs.acs.org/doi/10.1021/acs.jpcb.2c05258.

Simulation protocol, atomic charges from quantum calculations, protocols for applying the Q-model, and data analysis (PDF)

#### AUTHOR INFORMATION

#### **Corresponding Author**

Dmitry V. Matyushov — School of Molecular Sciences and Department of Physics, Arizona State University, Tempe, Arizona 85287-1504, United States; ⊚ orcid.org/0000-0002-9352-764X; Phone: (480)965-0057; Email: dmitrym@asu.edu

#### Author

Setare Mostajabi Sarhangi — School of Molecular Sciences and Department of Physics, Arizona State University, Tempe, Arizona 85287-1504, United States

Complete contact information is available at: https://pubs.acs.org/10.1021/acs.jpcb.2c05258

#### Votes

The authors declare no competing financial interest.

#### ACKNOWLEDGMENTS

This research was supported by the Army Research Office (ARO-W911NF2010320) and by the National Science Foundation (CHE-2154465). The supercomputer time was provided through Extreme Science and Engineering Discovery Environment (XSEDE) allocation MCB080071 and through ASU's Research Computing.

#### REFERENCES

- (1) Bostick, C. D.; Mukhopadhyay, S.; Pecht, I.; Sheves, M.; Cahen, D.; Lederman, D. Protein bioelectronics: a review of what we do and do not know. *Rep. Prog. Phys.* **2018**, *81*, 026601.
- (2) Zhang, B.; Ryan, E.; Wang, X.; Song, W.; Lindsay, S. Electronic transport in molecular wires of precisely controlled length built from modular proteins. *ACS Nano* **2022**, *16*, 1671–1680.
- (3) Eshel, Y.; Peskin, U.; Amdursky, N. Coherence-assisted electron diffusion across the multi-heme protein-based bacterial nanowire. *Nanotechnology* **2020**, *31*, 314002.
- (4) Dahl, P. J.; Yi, S. M.; Gu, Y.; Acharya, A.; Shipps, C.; Neu, J.; O'Brien, J. P.; Morzan, U. N.; Chaudhuri, S.; Guberman-Pfeffer, M. J.; et al. A 300-fold conductivity increase in microbial cytochrome nanowires due to temperature-induced restructuring of hydrogen bonding networks. *Sci. Adv.* 2022, *8*, eabm7193.
- (5) Stubbe, J.; Nocera, D. G.; Yee, C. S.; Chang, M. C. Y. Radical Initiation in the Class I Ribonucleotide Reductase: Long-Range Proton-Coupled Electron Transfer? *Chem. Rev.* **2003**, *103*, 2167–2202
- (6) Shih, C.; Museth, A. K.; Abrahamsson, M.; Blanco-Rodriguez, A. M.; Bilio, A. J. D.; Sudhamsu, J.; Crane, B. R.; Ronayne, K. L.; Towrie, M.; Vlček, A.; et al. Tryptophan-accelerated electron flow through proteins. *Science* **2008**, *320*, 1760–1762.
- (7) Bollinger, M. J. Electron relay in proteins. *Science* **2008**, 320, 1730–1731.
- (8) Shipps, C.; Kelly, H. R.; Dahl, P. J.; Yi, S. M.; Vu, D.; Boyer, D.; Glynn, C.; Sawaya, M. R.; Eisenberg, D.; Batista, V. S.; Malvankar, N. S. Intrinsic electronic conductivity of individual atomically resolved amyloid crystals reveals micrometer-long hole hopping via tyrosines. *Proc. Natl. Acad. Sci. U.S.A.* **2021**, *118*, e2014139118.
- (9) Gray, H. B.; Winkler, J. R. Functional and protective hole hopping in metalloenzymes. *Chem. Sci.* **2021**, *12*, 13988–14003.
- (10) Teo, R. D.; Wang, R.; Smithwick, E. R.; Migliore, A.; Therien, M. J.; Beratan, D. N. Mapping hole hopping escape routes in proteins. *Proc. Natl. Acad. Sci. U.S.A.* **2019**, *116*, 15811–15816.
- (11) Marcus, R. A.; Sutin, N. Electron transfer in chemistry and biology. *Biochim. Biophys. Acta* 1985, 811, 265–322.
- (12) Marcus, R. A. Electrostatic free energy and other properties of states having nonequilibrium polarization. I. *J. Chem. Phys.* **1956**, 24, 979–989.
- (13) Zwanzig, R.Nonequilibrium Statistical Mechanics; Oxford University Press: Oxford, 2001.
- (14) Nitzan, A.Chemical Dynamics in Condensed Phases: Relaxation, Transfer and Reactions in Condensed Molecular Systems; Oxford University Press: Oxford, 2006.
- (15) Chakrabarty, S.; Warshel, A. Capturing the energetics of water insertion in biological systems: The water flooding approach. *Proteins* **2013**, *81*, 93–106.
- (16) Bortolotti, C. A.; Amadei, A.; Aschi, M.; Borsari, M.; Corni, S.; Sola, M.; Daidone, I. The reversible opening of water channels in cytochrome c modulates the heme iron reduction potential. *J. Am. Chem. Soc.* **2012**, *134*, 13670–13678.
- (17) Martin, D. R.; Matyushov, D. V. Electron-transfer chain in respiratory complex I. Sci. Rep. 2017, 7, 5495.
- (18) Waskasi, M. M.; Martin, D. R.; Matyushov, D. V. Wetting of the protein active site leads to non-Marcusian reaction kinetics. *J. Phys. Chem. B* **2018**, *122*, 10490–10495.

- (19) Warshel, A. Dynamics of reactions in polar solvents. Semiclassical trajectory studies of electron-transfer and proton-transfer reactions. *J. Phys. Chem.* **1982**, *86*, 2218–2224.
- (20) Kuharski, R. A.; Bader, J. S.; Chandler, D.; Sprik, M.; Klein, M. L.; Impey, R. W. Molecular model for aqueous ferrous-ferric electron transfer. *J. Chem. Phys.* **1988**, *89*, 3248–3257.
- (21) Migliore, A.; Polizzi, N. F.; Therien, M. J.; Beratan, D. N. Biochemistry and theory of proton-coupled electron transfer. *Chem. Rev.* **2014**, *114*, 3381–3465.
- (22) Matyushov, D. V.; Voth, G. A. Modeling the free energy surfaces of electron transfer in condensed phases. *J. Chem. Phys.* **2000**, *113*, 5413.
- (23) Larson, B. C.; Pomponio, J. R.; Shafaat, H. S.; Kim, R. H.; Leigh, B. S.; Tauber, M. J.; Kim, J. E. Photogeneration and quenching of tryptophan radical in azurin. *J. Phys. Chem. B* **2015**, *119*, 9438–9449.
- (24) Zusman, L. D. Outer-sphere electron transfer in polar solvents. *Chem. Phys.* **1980**, *49*, 295–304.
- (25) Hynes, J. T. Outer-sphere electron-transfer reactions and frequency-dependent friction. J. Phys. Chem. 1986, 90, 3701–3706.
- (26) Rips, I.; Jortner, J. Dynamic solvent effects on outer-sphere electron transfer. J. Chem. Phys. 1987, 87, 2090–2104.
- (27) Yan, Y. J.; Sparpaglione, M.; Mukamel, S. Solvation dynamics in electron-transfer, isomerization, and nonlinear optical processes: a unified Liouville-space theory. *J. Phys. Chem.* **1988**, *92*, 4842–4853.
- (28) Matyushov, D. V. Dynamical effects in protein electrochemistry. J. Phys. Chem. B 2019, 123, 7290-7301.
- (29) Matyushov, D. V. Conformational dynamics modulating electron transfer. J. Chem. Phys. 2022, 157, 095102.
- (30) Bagchi, B. Molecular Relaxation in Liquids; Oxford University Press: Oxford, 2012.
- (31) Pal, S. K.; Zewail, A. H. Dynamics of water in biological recognition. *Chem. Rev.* **2004**, *104*, 2099–2123.
- (32) Zhang, L.; Yang, Y.; Kao, Y.-T.; Wang, L.; Zhong, D. Protein hydration dynamics and molecular mechanism of coupled water-protein fluctuations. *J. Am. Chem. Soc.* **2009**, *131*, 10677–10691.
- (33) Seyedi, S.; Waskasi, M. M.; Matyushov, D. V. Theory and electrochemistry of cytochrome c. J. Phys. Chem. B 2017, 121, 4958–4967.
- (34) Martin, D. R.; Matyushov, D. V. Communication: Microsecond dynamics of the protein and water affect electron transfer in a bacterial  $bc_1$  complex. J. Chem. Phys. **2015**, 142, 161101.
- (35) Murgida, D. H.; Hildebrandt, P. Proton-coupled electron transfer of cytochrome c. J. Am. Chem. Soc. 2001, 123, 4062–4068.
- (36) Wei, J. J.; Liu, H.; Niki, K.; Margoliash, E.; Waldeck, D. H. Probing electron tunneling pathways: Electrochemical study of rat heart cytochrome c and its mutant on pyridine-terminated SAMs. *J. Phys. Chem. B* **2004**, *108*, 16912–16917.
- (37) Murgida, D. H.; Hildebrandt, P. Redox and redox-coupled processes of heme proteins and enzymes at electrochemical interfaces. *Phys. Chem. Chem. Phys.* **2005**, *7*, 3773–3784.
- (38) Monari, S.; Battistuzzi, G.; Bortolotti, C. A.; Yanagisawa, S.; Sato, K.; Li, C.; Salard, I.; Kostrz, D.; Borsari, M.; Ranieri, A.; et al. Understanding the mechanism of short-range electron transfer using an immobilized cupredoxin. *J. Am. Chem. Soc.* **2012**, *134*, 11848–11851.
- (39) Zitare, U. A.; Szuster, J.; Santalla, M. C.; Morgada, M. N.; Vila, A. J.; Murgida, D. H. Dynamical effects in metalloprotein heterogeneous electron transfer. *Electrochim. Acta* **2020**, 342, 136095.
- (40) Page, C. C.; Moser, C. C.; Chen, X. X.; Dutton, P. L. Natural engineering principles of electron tunneling in biological oxidation-reduction. *Nature* **1999**, 402, 47–52.
- (41) Page, C. C.; Moser, C. C.; Dutton, P. L. Mechanism for electron transfer within and between proteins. *Curr. Opinion in Biology* **2003**, *7*, 551.
- (42) Moser, C. C.; Anderson, J. R.; Dutton, P. L. Guidelines for tunneling in enzymes. *Biochim. Biophys. Acta Bioenergetics* **2010**, 1797, 1573–1586.

- (43) Waldeck, D. H.; Khoshtariya, D. E. Applications of Electrochemistry and Nanotechnology in Biology and Medicine I; Springer New York: New York, NY, 2011pp 105–238.
- (44) Feynman, R. P.; Leighton, R. B.; Sands, M. The Feynman lectures on physics, Vol. I: Mainly mechanics, radiation, and heat; Addison-Wesley: Reading, MA, 1963.
- (45) LeBard, D. N.; Matyushov, D. V. Protein-water electrostatics and principles of bioenergetics. *Phys. Chem. Chem. Phys.* **2010**, *12*, 15335–15348.
- (46) Small, D. W.; Matyushov, D. V.; Voth, G. A. The theory of electron transfer: What may be missing? *J. Am. Chem. Soc.* **2003**, *125*, 7470–7478.
- (47) Bennett, C. H. Efficient estimation of free energy differences from Monte Carlo data. *J. Comput. Phys.* **1976**, 22, 245–268.
- (48) Tachiya, M. Relation between the electron-transfer rate and the free energy change of reaction. *J. Phys. Chem.* **1989**, *93*, 7050–7052.
- (49) Matyushov, D. V. Protein electron transfer: is biology (thermo)dynamic? J. Phys.: Condens. Matter 2015, 27, 473001.
- (50) Nagel, Z. D.; Dong, M.; Bahnson, B. J.; Klinman, J. P. Impaired protein conformational landscapes as revealed in anomalous Arrhenius prefactors. *Proc. Natl. Acad. Sci. U.S.A.* **2011**, *108*, 10520–10525.
- (51) Kurchan, J. In and out of equilibrium. *Nature* **2005**, 433, 222–225.
- (52) Barragan, A. M.; Soudackov, A. V.; Luthey-Schulten, Z.; Hammes-Schiffer, S.; Schulten, K.; Solov'yov, I. A. Theoretical description of the primary proton-coupled electron transfer reaction in the cytochrome bc<sub>1</sub> complex. *J. Am. Chem. Soc.* **2021**, *143*, 715–723
- (53) Frauenfelder, H. In *The Physics of proteins. An introduction to biological physics and molecular biophysics*; Chan, S. S., Chan, W. S., Ed.; Springer: New York, 2010.
- (54) Sarhangi, S. M.; Matyushov, D. V. Anomalously small reorganization energy of half redox reaction of azurin. *J. Phys. Chem. B* **2022**, *126*, 3000–3011.
- (55) Kontkanen, O. V.; Biriukov, D.; Futera, Z. Reorganization free energy of copper proteins in solution, in vacuum, and on metal surfaces. *J. Chem. Phys.* **2022**, *156*, 175101.
- (56) Guberman-Pfeffer, M. J. Heme hopping falls short: What explains anti-Arrhenius conductivity in a multi-heme cytochrome nanowire. *bioRxiv* **2022**, No. 2022.08.01.502099.
- (57) Fried, S. D.; Bagchi, S.; Boxer, S. G. Extreme electric fields power catalysis in the active site of ketosteroid isomerase. *Science* **2014**, 346, 1510–1514.
- (58) Adman, E.; Jensen, L. Structural features of azurin at 2.7 Å resolution. *Israel J. Chem.* **1981**, 21, 8–12.
- (59) Bernini, C.; Pogni, R.; Ruiz-Duenas, F. J.; Martínez, A. T.; Basosi, R.; Sinicropi, A. EPR parameters of amino acid radicals in P. eryngii versatile peroxidase and its W164Y variant computed at the QM/MM level. *Phys. Chem. Chem. Phys.* **2011**, *13*, 5078–5098.
- (60) Phillips, J. C.; Hardy, D. J.; Maia, J. D. C.; Stone, J. E.; Ribeiro, J. V.; Bernardi, R. C.; Buch, R.; Fiorin, G.; Hénin, J.; Jiang, W.; et al. Scalable molecular dynamics on CPU and GPU architectures with NAMD. *J. Chem. Phys.* **2020**, *153*, 044130.
- (61) Dinpajooh, M.; Martin, D. R.; Matyushov, D. V. Polarizability of the active site of cytochrome c reduces the activation barrier for electron transfer. *Sci. Rep.* **2016**, *6*, 28152.
- (62) Garner, D. K.; Vaughan, M. D.; Hwang, H. J.; Savelieff, M. G.; Berry, S. M.; Honek, J. F.; Lu, Y. Reduction potential tuning of the blue copper center in Pseudomonas Aeruginosa azurin by the axial methionine as probed by unnatural amino acids. *J. Am. Chem. Soc.* **2006**, *128*, 15608–15617.
- (63) Glover, S. D.; Tyburski, R.; Liang, L.; Tommos, C.; Hammarström, L. Pourbaix diagram, proton-coupled electron transfer, and decay kinetics of a protein tryptophan radical: Comparing the redox properties of W32 \* and Y32 \* generated inside the structurally characterized  $\alpha_3$ W and  $\alpha_3$ Y proteins. *J. Am. Chem. Soc.* **2018**, *140*, 185–192.

- (64) Tyson, K. J.; Davis, A. N.; Norris, J. L.; Bartolotti, L. J.; Hvastkovs, E. G.; Offenbacher, A. R. Impact of local electrostatics on the redox properties of tryptophan radicals in azurin: Implications for redox-active tryptophans in proton-coupled electron transfer. *J. Phys. Chem. Lett.* **2020**, *11*, 2408–2413.
- (65) Voityuk, A. A. Electron transfer between [4Fe-4S] clusters. Chem. Phys. Lett. 2010, 495, 131–134.
- (66) Teo, R. D.; Rousseau, B. J.G.; Smithwick, E. R.; Di Felice, R.; Beratan, D. N.; Migliore, A. Charge transfer between [4Fe4S] proteins and DNA is unidirectional: Implications for biomolecular signaling. *Chem.* **2019**, *5*, 122–137.
- (67) Hopfield, J. J. Electron transfer between biological molecules by thermally activated tunneling. *Proc. Nat. Acad. Sci.* **1974**, 71, 3640.
- (68) Gray, H. B.; Winkler, J. R. Long-range electron transfer. *Proc. Natl. Acad. Sci. U. S. A.* **2005**, *102*, 3534–3539.
- (69) Shafaat, H. S.; Leigh, B. S.; Tauber, M. J.; Kim, J. E. Spectroscopic comparison of photogenerated tryptophan radicals in azurin: Effects of local environment and structure. *J. Am. Chem. Soc.* **2010**, *132*, 9030–9039.
- (70) Consani, C.; Aubock, G.; van Mourik, F.; Chergui, M. Ultrafast tryptophan-to-heme electron transfer in myoglobins revealed by UV 2D spectroscopy. *Science* **2013**, 339, 1586–1589.
- (71) Aubert, C.; Vos, M. H.; Mathis, P.; Eker, A. P. M.; Brettel, K. Intraprotein radical transfer during photoactivation of DNA photolyase. *Nature* **2000**, *405*, 586–590.
- (72) Gaines, J. C.; Clark, A. H.; Regan, L.; O'Hern, C. S. Packing in protein cores. J. Phys.: Condens. Matter 2017, 29, 293001–16.
- (73) Jäckel, C.; Kast, P.; Hilvert, D. Protein design by directed evolution. *Annu. Rev. Biophys.* **2008**, *37*, 153–173.
- (74) Nicholls, D. G.; Ferguson, S. J.Bioenergetics4; Academic Press: Amsterdam, 2013.
- (75) Gray, H. B.; Winkler, J. R. Electron tunneling through proteins. Q. Rev. Biophys. 2003, 36, 341–372.
- (76) Pauling, L. Molecular architecture and biological reactions. Chem. Eng. News 1946, 24, 1375–1377.
- (77) Amyes, T. L.; Richard, J. P. Specificity in transition state binding: The Pauling model revisited. *Biochem* **2013**, *52*, 2021–2035.
- (78) Rasaiah, J. C.; Garde, S.; Hummer, G. Water in nonpolar confinement: From nanotubes to proteins and beyond. *Annu. Rev. Phys. Chem.* **2008**, *59*, 713–740.
- (79) Fried, S. D. E.; Hewage, K. S. K.; Eitel, A. R.; Struts, A. V.; Weerasinghe, N.; Perera, S. M. D. C.; Brown, M. F. Hydration-mediated G-protein-coupled receptor activation. *Proc. Natl. Acad. Sci. U.S.A.* 2022, 119, e2117349119.
- (80) Jimenez, R.; Fleming, G. R.; Kumar, P. V.; Maroncelli, M. Femtosecond solvation dynamics of water. *Nature* **1994**, *369*, 471–473.
- (81) Yue, H.; Khoshtariya, D.; Waldeck, D. H.; Grochol, J.; Hildebrandt, P.; Murgida, D. H. On the electron transfer mechanism between cytochrome c and metal electrodes. Evidence for dynamic control at short distances. *J. Phys. Chem. B* **2006**, *110*, 19906–19913.
- (82) Alvarez-Paggi, D.; Zitare, U.; Murgida, D. H. The role of protein dynamics and thermal fluctuations in regulating cytochrome c/cytochrome c oxidase electron transfer. *Biochim. Biophys. Acta Bioenergetics* **2014**, 1837, 1196–1207.
- (83) Moser, C. C.; Keske, J. M.; Warncke, K.; Farid, R. S.; Dutton, P. L. Nature of biological electron transfer. *Nature* **1992**, 355, 796–802.
- (84) LeBard, D. N.; Kapko, V.; Matyushov, D. V. Energetics and kinetics of primary charge separation in bacterial photosynthesis. *J. Phys. Chem. B* **2008**, *112*, 10322–10342.
- (85) Lu, Y.; Kundu, M.; Zhong, D. Effects of nonequilibrium fluctuations on ultrafast short-range electron transfer dynamics. *Nat. Commun.* **2020**, *11*, 265–9.
- (86) Yang, J.; Zhang, Y.; Lu, Y.; Wang, L.; Lu, F.; Zhong, D. Ultrafast dynamics of nonequilibrium short-range electron transfer in semiquinone flavodoxin. *J. Phys. Chem. Lett.* **2022**, *13*, 3202–3208.
- (87) Wang, H.; Lin, S.; Allen, J. P.; Williams, J. C.; Blankert, S.; Laser, C.; Woodbury, N. W. Protein dynamics control the kinetics of

- initial electron transfer in photosynthesis. Science 2007, 316, 747-750
- (88) Lovley, D. R. Electrically conductive pili: Biological function and potential applications in electronics. *Curr. Opin. Electrochem* **2017**, *4*, 190–198.
- (89) Gu, Y.; Srikanth, V.; Salazar-Morales, A. I.; Jain, R.; O'Brien, J. P.; Yi, S. M.; Soni, R. K.; Samatey, F. A.; Yalcin, S. E.; Malvankar, N. S. Structure of Geobacter pili reveals secretory rather than nanowire behaviour. *Nature* **2021**, *597*, 430–434.
- (90) Ru, X.; Zhang, P.; Beratan, D. N. Assessing possible mechanisms of micrometer-scale electron transfer in heme-free Geobacter sulfurreducens pili. *J. Phys. Chem. B* **2019**, *123*, 5035–5047.
- (91) Yalcin, S. E.; Malvankar, N. S. The blind men and the filament: Understanding structures and functions of microbial nanowires. *Cur. Opin. Chem. Biol.* **2020**, *59*, 193–201.

### Recommended by ACS

#### Ergodicity Breaking in Thermal Biological Electron Transfer? Cytochrome C Revisited II

Zdenek Futera, Jochen Blumberger, et al.

MARCH 30, 2020

THE JOURNAL OF PHYSICAL CHEMISTRY B

READ [7]

# Unexpected Heme Redox Potential Values Implicate an Uphill Step in Cytochrome $b_k f$

Mateusz Szwalec, Artur Osyczka, et al.

NOVEMBER 18, 2022

THE JOURNAL OF PHYSICAL CHEMISTRY B

READ 🗹

# The Role of Hydrophobicity in the Stability and pH-Switchability of $(RXDX)_4$ and $Coumarin-(RXDX)_4$ Conjugate $\beta$ -Sheets

Ryan Weber and Martin McCullagh

FEBRUARY 11, 2020

THE JOURNAL OF PHYSICAL CHEMISTRY B

READ 🗹

## Force Response of Polypeptide Chains from Water-Explicit MD Simulations

Richard Schwarzl, Roland R. Netz, et al.

JUNE 12, 2020

MACROMOLECULES

READ 🗹

Get More Suggestions >